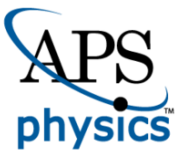

Active Contact Forces Drive Nonequilibrium Fluctuations in Membrane Vesicles

Sho C. Takatori and Amaresh Sahu

Phys. Rev. Lett. **124**, 158102 — Published 16 April 2020

DOI: 10.1103/PhysRevLett.124.158102

Active Contact Forces Drive Non-Equilibrium Fluctuations in Membrane Vesicles

Sho C. Takatori[1, *] and Amaresh Sahu[2, ‡]

[1] *Department of Chemical Engineering, University of California, Santa Barbara, Santa Barbara, CA 93106*
[2] *Department of Chemical & Biomolecular Engineering, University of California, Berkeley 94720, USA*

(Dated: March 20, 2020)

We analyze the non-equilibrium shape fluctuations of giant unilamellar vesicles encapsulating motile bacteria. Owing to bacteria–membrane collisions, we experimentally observe a significant increase in the magnitude of membrane fluctuations at low wave numbers, compared to the well-known thermal fluctuation spectrum. We interrogate these results by numerically simulating membrane height fluctuations via a modified Langevin equation, which includes bacteria–membrane contact forces. Taking advantage of the length and time scale separation of these contact forces and thermal noise, we further corroborate our results with an approximate theoretical solution to the dynamical membrane equations. Our theory and simulations demonstrate excellent agreement with non-equilibrium fluctuations observed in experiments. Moreover, our theory reveals that the fluctuation–dissipation theorem is not broken by the bacteria; rather, membrane fluctuations can be decomposed into thermal and active components.

Biological lipid membranes make up the boundary of the cell, and act as a dynamic barrier between the cell's internal contents and extracellular environment. Such membranes are acted upon by a variety of so-called active forces—including those from transmembrane protein pumps [1, 2] and the underlying cytoskeleton [3, 4]. There have been considerable experimental [5, 6] and theoretical [7–19] efforts to show how active forces from transmembrane proteins and the cytoskeleton cause membrane fluctuations to deviate from the well-known equilibrium result, with a particular emphasis on the membranes of red blood cells [20–25]. More recently, there has been growing interest in analyzing the behavior of self-propelled active colloids enclosed within membrane vesicles [26–30], as such systems can serve as a useful minimal model of the cell.

In this Letter, we experimentally and theoretically study the membrane shape fluctuations induced by motile bacteria enclosed within giant unilamellar vesicles (GUVs). A schematic of our experimental system, as well as fluorescence microscopy images involving motile and nonmotile bacteria, are shown in Fig. 1; see also Vids. S1–S5 in the Supplemental Material (SM) [31]. We observe motile, micron-sized bacteria pushing against their elastic membrane container and causing large deformations until they reorient after ∼0.5 seconds and swim in another direction. As shown by the filled brown (passive) and open black (active) circles in Fig. 2, as well as Fig. 1 of the SM [31], the bacteria cause a significant change in the distribution of membrane deflections and the corresponding fluctuation spectrum. Due to the separation in length and time scales of bacteria–membrane contact

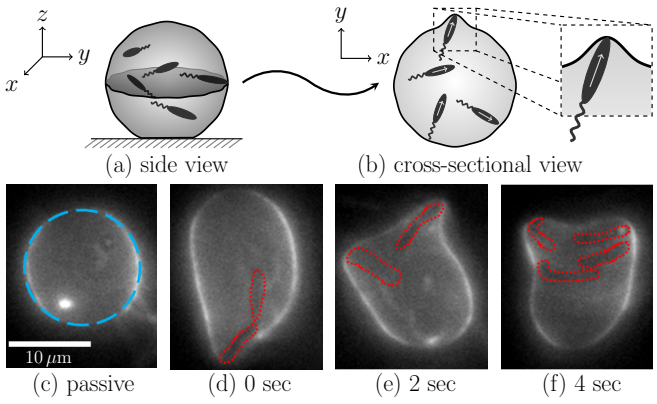

(a) side view (b) cross-sectional view

(c) passive (d) 0 sec (e) 2 sec (f) 4 sec

FIG. 1. Giant unilamellar vesicle (GUV) containing motile *Bacillus subtilis* PY79. The schematic shows how the three-dimensional system (a) is imaged at a single equatorial cross-section (b) to generate the experimental images in (c)–(f). The dashed blue outline in (c) shows the undeformed spherical shape of the membrane when bacteria are non-motile, while (d)–(f) show how motile bacteria (dotted red outlines) generate large membrane deformations at different times.

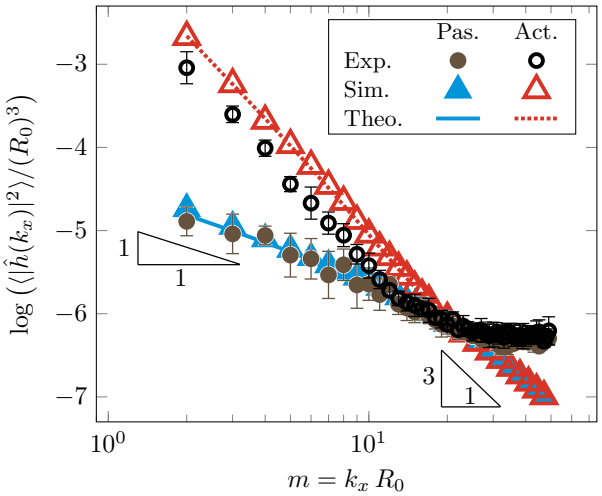

FIG. 2. Membrane height fluctuations, $\langle|\hat{h}(k_x)|^2\rangle$, for passive (brown, blue) and active (black, red) vesicles, as a function of the mode $m = k_x R_0$. Results are shown from experiments (circles), numerical simulations (triangles, see Eq. 3), and analytical theory (lines, see Eq. 6). Both simulations and theory show excellent agreement with experiments, in the absence of any fitting parameters.

and equilibrium fluctuations, our active fluctuation spectrum only deviates from its passive counterpart at small wave numbers. Figure 2 also presents our main quantitative result, as we find excellent agreement between experiments (circles), simulations (triangles), and analytical theory (curves). We now provide a brief summary of the experimental protocol used to construct the 'active vesicles' of Fig. 1 before describing the simulations and analytical theory used to generate Fig. 2.

Experiments.—A modified electroformation protocol [32, 33] was used to encapsulate *Bacillus subtilis* PY79 inside GUVs. A 4 mg/mL stock solution of 99.5% 1,2-dioleoyl-sn-glycero-3-phosphocholine (DOPC) and 0.5% L-α-phosphatidylethanolamine-N-lissamine rhodamine B sulfonyl (Egg Liss Rhod PE) dissolved in chloroform was spin-coated onto indium tin oxide (ITO) coated glass slides with surface resistivity of ~ 50–$100\ \Omega$/sq. Luria broth nutrient medium was placed between the ITO slides with a spacer and connected to a wavefunction generator. After 75–90 minutes of a square wave with 1 V_{pp} at 10 Hz, a small volume of a dense suspension of an overnight culture of PY79 was added between the ITO slides and set aside in the absence of voltage for 10–15 minutes with the lipid-coated ITO slide facing down. Finally, we applied 20 minutes of a square wave with 0.3 V_{pp} at 2 Hz. The suspension was imaged on an inverted widefield fluorescence microscope at 30°C.

Prior to electroformation, the bacteria are not highly motile, as the overnight culture is in a stationary growth phase. During electroformation, however, *B. subtilis* is introduced into the chamber with fresh nutrient medium; the bacteria become motile after ~ 30 min [34]. Immediately after electroformation, we identify and image a vesicle containing several nonmotile bacteria to measure the undeformed vesicle radius and the membrane height fluctuations—which correspond to those of a vesicle without bacteria, and which we refer to as a 'passive vesicle' (see Fig. 1c). Once the bacteria become motile, we measure the membrane fluctuations of the same vesicle [35]. In this way, we are able to directly compare passive and active membrane fluctuations of a single vesicle both visually (Fig. 1c–f and Vids. S1–S5 in the SM [31]) and in Fourier space (Fig. 2, filled brown and open black circles). We analyze the membrane fluctuation spectra of passive and active vesicles using standard methods [36–38], in which we have removed the $m = 1$ mode due to experimental difficulties in locating the center of the vesicle [39]. We note that experimental data at large wave numbers level off due to limitations in the camera resolution, whereas our simulations (described subsequently) capture the full spectrum. Moreover, as we are experimentally capturing fluctuations at only a single cross-section of the membrane vesicle (see Fig. 1), when computing the Fourier spectrum we are implicitly averaging over one of the two independent Fourier modes [36].

Development of the theory.—We have so far experimentally demonstrated how active particles, in this case *B. subtilis*, cause dramatic changes to the fluctuation spectrum of the surrounding lipid membrane. However, the physics underlying such interactions remains unclear. In particular, while other works have considered active forces arising from transmembrane proteins [7–16] or simulated active particles in vesicles [26–29], there is no theoretical description of our experimental results. Thus, to better understand our experimental system, we both theoretically and numerically model membrane fluctuations in the presence of active particles. Both of these developments rely on the so-called Monge parametrization of the membrane [40], which treats the membrane as a nearly flat plane with small height perturbations, to avoid the complex equations describing a perturbed spherical membrane [41]. Despite this rather severe simplification, the agreement between our experiments, simulations, and theory in the absence of any fitting parameters indicates our simple model captures the essential physics of particle–membrane contact.

In thermal equilibrium, the height fluctuations of a nearly planar membrane described by a Helfrich [42–44] Hamiltonian $\mathcal{H} = \frac{1}{2}\int \kappa(\nabla^2 h)^2 + \lambda(\nabla h)^2\,\mathrm{d}x\,\mathrm{d}y$ are given by $\langle|\hat{h}(\boldsymbol{k})|^2\rangle_{\mathrm{pas}} = k_{\mathrm{B}}T/(\kappa k^4 + \lambda k^2)$, where $\boldsymbol{k} = (k_x, k_y)$ is the wave vector conjugate to position $\boldsymbol{x} = (x, y)$, $k_{\mathrm{B}}T$ is the thermal energy, κ is the membrane bending modulus, and λ is the surface tension (κ and λ are assumed to be constant). In our experiments, however, the vesicles are only imaged at a single cross section (Fig. 1). Thus, to compare experiments and theory, we average the theoretical fluctuation spectrum over k_y modes to find $\langle|\hat{h}(k_x)|^2\rangle_{\mathrm{pas}} = (k_x^{-1} - (k_x^2 + \lambda/\kappa)^{-1/2}) \cdot k_{\mathrm{B}}T/(2\lambda)$; details are provided in the SM [31]. As shown in Fig. 2, passive experimental data (brown circles) agree with the theoretical prediction, $\langle|\hat{h}(k_x)|^2\rangle_{\mathrm{pas}}$, for the choice $\kappa = 14.3\ k_{\mathrm{B}}T$ and $\lambda = 4 \cdot 10^{-3}$ pN/nm (blue curve). We fixed these parameters in all of our active membrane calculations, and additionally found our numerical and theoretical active results are insensitive to our choice of κ and λ [31].

Equilibrium techniques cannot describe active vesicle fluctuations due to the presence of non-conservative contact forces, so we turn to a dynamical membrane description. The Langevin equation governing membrane shape changes is given by [12, 17, 45]

$$\frac{\partial h(\boldsymbol{x},t)}{\partial t} = \eta(\boldsymbol{x},t) + \int \mathrm{d}\boldsymbol{x}' \left[\Lambda(\boldsymbol{x}-\boldsymbol{x}')\, p^{\mathrm{tot}}(\boldsymbol{x}',t)\right], \quad (1)$$

where h is the membrane height, η is Gaussian white noise satisfying the fluctuation–dissipation theorem, $\Lambda(\boldsymbol{x}-\boldsymbol{x}') := (8\pi\mu|\boldsymbol{x}-\boldsymbol{x}'|)^{-1}$ is the $\boldsymbol{e}_z \otimes \boldsymbol{e}_z$ component of the Oseen tensor for a Newtonian fluid with viscosity μ, and $-p^{\mathrm{tot}}\boldsymbol{e}_z$ is the total force per area exerted on the membrane by the surrounding fluid. In this case, $p^{\mathrm{tot}} = p^{\mathrm{int}} + p^{\mathrm{act}}$, where the internal membrane force per

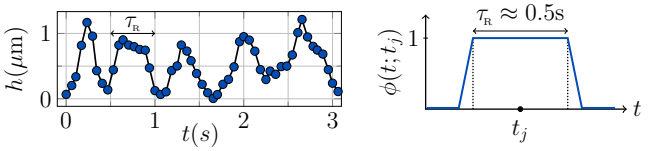

(a) experiment (b) simulation

FIG. 3. Temporal nature of the bacteria–vesicle collisions. (a) Magnitude of the radial deflection of the vesicle at a single location, in a single experiment, as a function of time. The trapezoid shape is characteristic of a bacteria pushing against the membrane for reorientation time τ_R; smaller peaks indicate a bacteria sliding along the membrane surface. (b) Numerical approximation of a head-on collision's temporal component, called $\phi(t;t_j)$. The modified step function is centered at the collision time t_j.

area $p^{\text{int}} := -\delta\mathcal{H}/\delta h = -\kappa\nabla^4 h + \lambda\nabla^2 h$, and p^{act} is the force per area due to active particles (see SM [31] for details).

To approximate p^{act}, we model the bacteria as self-propelled particles of half-width a which randomly collide with the membrane vesicle. For N_c total collisions between the various bacteria and the membrane, where the j^{th} collision occurs at location $\boldsymbol{x}_j$ and time t_j, the active force per area on the membrane at location $\boldsymbol{x}$ and time t is given by

$$p^{\text{act}}(\boldsymbol{x},t) = \sum_{j=1}^{N_c} \bar{p}\,\phi(t;t_j)\,\exp\left\{-\frac{(\boldsymbol{x}-\boldsymbol{x}_j)^2}{2a^2}\right\}. \tag{2}$$

In Eq. (2), $\bar{p}$ is the maximum pressure the bacteria exerts on the membrane, which we estimate to be equal to the pressure exerted by a membrane on a spherical particle of radius a, $\bar{p} \approx 2\lambda/a$. Furthermore, as shown in Fig. 3, $\phi(t;t_j)$ is a modified step function centered at time t_j which captures the temporal nature of the collision. In choosing ϕ, we approximated a bacterium as initially traveling at velocity U_0 towards the membrane, coming to rest due to elastic membrane forces, and remaining there for reorientation time τ_R before swimming back into the interior of the vesicle. Finally, the exponential term in Eq. (2) is a simple model of the finite size of the particle, which spreads the contact force over a portion of the membrane and is amenable to numerical computation.

At this point, we highlight that all details of the bacteria–membrane interactions are modeled through $\bar{p}$, $\phi(t;t_j)$, and the exponential spreading of the contact force, such that Eq. (2) contains the main difference between the present work and other theoretical developments of active membranes [7–19]. In particular, when active forces arise from membrane–protein interactions, there is no length or time scale separation between active and thermal forces. As a result, the non-equilibrium fluctuation spectrum can often be obtained by renormalizing the temperature [5–9, 12, 18]. In our case, however, bacteria–membrane interactions are much slower than equilibrium fluctuations, as captured by ϕ, and are spread over much larger distances, as captured by the Gaussian in Eq. (2). Note that in our model, for simplicity we neglect the complex hydrodynamic interactions between bacteria and membrane, as well as any permeability effects from fluid passing through the membrane. As experimental investigations found a rapidly decaying flow field for bacteria close to surfaces [46], we simply choose to capture all bacteria–membrane interactions in the active pressure term p^{act}.

Numerical solution.—Using standard techniques [12, 17, 45], we take the Fourier transform of Eq. (1) and recognize the Fourier modes are independent. For each wave vector $\boldsymbol{k} = (m,n)/R_0$, where $m,n \in \mathbb{Z}$ and R_0 is the unperturbed vesicle radius, the corresponding evolution equation is given by [31]

$$\frac{\partial \hat{h}(\boldsymbol{k},t)}{\partial t} = -\omega(k)\,\hat{h}(\boldsymbol{k},t) + \hat{\eta}(\boldsymbol{k},t) + L\hat{\Lambda}(\boldsymbol{k})\,\hat{p}^{\text{act}}(\boldsymbol{k},t)\,. \tag{3}$$

In Eq. (3), $\omega(k) := (\kappa k^3 + \lambda k)/(4\mu)$ is the relaxation frequency of mode $\boldsymbol{k}$, $L = 2\pi R_0$ is the length of the planar membrane patch, $\hat{\Lambda}(\boldsymbol{k}) = (4\mu k L)^{-1}$ is the Fourier transform of $\Lambda(\boldsymbol{x})$, and $\hat{p}^{\text{act}}(\boldsymbol{k},t)$ is the Fourier transform of the active force per area (2). The last term in Eq. (3) is given by

$$L\hat{\Lambda}(\boldsymbol{k})\,\hat{p}^{\text{act}} = \sum_{j=1}^{N_c} \frac{a^2\,\bar{p}}{4\mu k R_0}\,\phi(t;t_j)\,\exp\left\{-i\boldsymbol{x}_j\cdot\boldsymbol{k} - \frac{a^2\,k^2}{2}\right\}. \tag{4}$$

We discretize the height evolution equation (3) as shown in the SM [31] and compute $\hat{h}(\boldsymbol{k},t)$ for all $\boldsymbol{k}$, from which we calculate the height fluctuations. After integrating over k_y, we plot our simulation results as the triangles in Fig. 2 for the passive (filled blue) and active (open red) cases. Passive results were calculated by setting $\hat{p}^{\text{act}} = 0$ in Eq. (3). While such techniques are known to attain the passive fluctuation spectrum [12, 17, 45], we see excellent agreement between active experiments and simulations as well [47]. Furthermore, there are no fitting parameters in our development: κ and λ are found from the membrane fluctuations before bacteria become motile, the viscosity μ of the fluid is known, $R_0 = 4\,\mu$m is the undeformed vesicle radius, the bacteria have a reorientation time $\tau_R \approx 0.5$ sec, and $a = 0.25\,\mu$m is half the average width of a bacterium.

Analytical solution.—To develop an analytical expression for the active membrane fluctuation spectrum, we first consider Eqs. (3) and (4) for a vesicle containing a single active particle. By approximating $\phi(t;t_j)$ as being either 0 or 1 (see Fig. 3b), the membrane is either fully separated from ($\phi = 0$) or fully in contact with ($\phi = 1$) the bacterium. When there is no contact, the membrane feels thermal perturbations, such that its height fluctuations are given by the passive result. If there is contact (denoted with a subscript 'c'), the mem-

brane again feels thermal perturbations, but this time oscillates about some nonzero value—which we denote $\bar{h}(\boldsymbol{k})$. In this case, as the time scales of the two processes are separated and the thermal background is independent of the active forces, the height fluctuations are given by $\langle|\hat{h}(\boldsymbol{k})|^2\rangle_{\rm c} = \langle|\hat{h}(\boldsymbol{k})|^2\rangle_{\rm pas} + |\bar{h}(\boldsymbol{k})|^2$. We assume a single bacterium spends reorientation time $\tau_{\rm R}$ in contact with the membrane, then travels for time $\tau_{\rm T}$ in the interior of the vesicle, and repeats. Thus, for a single particle, $\langle|\hat{h}(\boldsymbol{k})|^2\rangle = \langle|\hat{h}(\boldsymbol{k})|^2\rangle_{\rm pas} + |\bar{h}(\boldsymbol{k})|^2\,\tau_{\rm R}/(\tau_{\rm R}+\tau_{\rm T})$. When there are $N_{\rm p}$ particles in the vesicle, we assume they are non-interacting, such that the membrane height fluctuations are given by

$$\langle|\hat{h}(\boldsymbol{k})|^2\rangle \;=\; \frac{k_{\rm B}T}{\kappa k^4+\lambda k^2} \;+\; \frac{N_{\rm p}\,\tau_{\rm R}}{\tau_{\rm R}+\tau_{\rm T}}\,|\bar{h}(\boldsymbol{k})|^2\;. \qquad (5)$$

Thus, by determining $|\bar{h}(\boldsymbol{k})|^2$, we determine the membrane fluctuation spectrum of a bacteria-containing lipid membrane vesicle.

To calculate $\bar{h}(\boldsymbol{k})$, we average Eq. (3) in time for the case of a single bacterium, when there is contact ($\phi = 1$). The time derivative and thermal noise terms average to zero, and $\bar{h}(\boldsymbol{k})$ is the average value of $\hat{h}(\boldsymbol{k},t)$. Thus, by solving for $\bar{h}(\boldsymbol{k})$ and substituting into Eq. (5), we obtain

$$\langle|\hat{h}(\boldsymbol{k})|^2\rangle = \frac{k_{\rm B}T}{\kappa k^4+\lambda k^2} \;+\; \frac{N_{\rm p}\,\tau_{\rm R}}{\tau_{\rm T}+\tau_{\rm R}}\left(\frac{a^2\,\bar{p}/R_0}{\kappa k^4+\lambda k^2}\right)^2 {\rm e}^{-a^2k^2}\;. \qquad (6)$$

Equation (6) is our main theoretical result. As shown by the dotted red curve in Fig. 2, Eq. (6) demonstrates excellent agreement with the experiments and active simulations—again without any fitting parameters. Here, the membrane contains $N_{\rm p} \approx 7$ bacteria, and we estimate $\tau_{\rm T} \approx 2R_0/U_0 \approx 0.5$ sec as the time for a bacterium to travel the vesicle diameter, moving at speed $U_0 \approx 15$ μm/sec. We believe our simulations and theory consistently over-predict experimental results because we neglect bacteria–bacteria collisions within the vesicle. Including such collisions would decrease the number of bacteria–membrane collisions $N_{\rm c}$ in simulations (4), and reduce the proportion of time bacteria are in contact with the membrane in our analytical result (6), both of which would slightly decrease the magnitude of active height fluctuations predicted by theory and simulation.

To test the robustness of our theoretical model, we analyze two additional active vesicles, which are different sizes and contain different numbers of bacteria. As shown in the SM [31], our theory and simulations again demonstrate excellent agreement with experiments when $R_0 \approx 8$ μm and $N_{\rm p} \approx 10$, and good agreement when $R_0 \approx 15$ μm and $N_{\rm p} \approx 20$. In the latter case with many bacteria, there are often times when multiple bacteria contact a local portion of the membrane in quick succession—thus violating our assumption of independent bacterial collisions. Such behavior, which is well-known in the study of active particles near surfaces [48, 49], effectively converts longer wavelength fluctuations into shorter wavelength ones, and qualitatively changes the shape of the active fluctuation spectrum. We recognize one measure of particle–particle effects at the vesicle boundary is the dimensionless parameter $N_{\rm p}\,\tau_{\rm R}/(\tau_{\rm T}+\tau_{\rm R})$ appearing in Eq. (6). In cases where the agreement between experiments and theory is excellent, we calculate $N_{\rm p}\,\tau_{\rm R}/(\tau_{\rm T}+\tau_{\rm R}) \approx 3.4$ for the vesicle in Fig. 2 and $N_{\rm p}\,\tau_{\rm R}/(\tau_{\rm T}+\tau_{\rm R}) \approx 3.2$ for the 10-particle vesicle in the SM [31]. In the case where particle–particle correlations become significant at the membrane, however, $N_{\rm p}\,\tau_{\rm R}/(\tau_{\rm T}+\tau_{\rm R}) \approx 4.0$—which seems to approach the upper limit of our theory's validity. Thus, we conclude that our theory and simulations are valid in the low-particle regime when $N_{\rm p}\,\tau_{\rm R}/(\tau_{\rm T}+\tau_{\rm R}) \lesssim 4$.

Conclusions.—Equation (6) concludes our theoretical and numerical efforts. With an analytical expression for the membrane fluctuation spectrum which closely matches experiments, we make several observations regarding the physics of lipid membrane systems driven by active contact forces. First, Eqs. (5) and (6) show the fluctuation–dissipation theorem is not broken. Instead, thermal noise continues to excite all height modes, while active forces dominate small modes. Intuitively, active contact forces only excite long wavelength modes due to the finite size of a single bacterium, and the distribution of the contact force over a large area. In fact, the exponential contact term in Eq. (6) is the main difference between the present work and those concerned with active fluctuations of transmembrane proteins [8, 10, 16]: by setting the protein timescale to be large in the latter, one recovers an expression similar to Eq. (6)—however without the exponential term. Additionally, our analytical result (6) demonstrates the active fluctuation spectrum does not follow a power-law behavior at low $\boldsymbol{k}$, and for this reason we do not provide a scaling relation in the active region of Fig. 2. Importantly, our theory and simulations took advantage of the time and length scale separation between active contact and equilibrium forces, and as a result we were able to capture the essential membrane physics using simple techniques. We note that our theoretical prediction is robust to variations in bacterial and membrane properties, as demonstrated by our sensitivity analysis in the SM [31].

We end this Letter by providing two avenues for future directions. First, our experimental method can be easily adapted to encapsulate different types of active particles. As one example, we synthesized active Janus particles as in Ref. [50], encapsulated them in lipid membrane vesicles using similar experimental methods, and induced them to propel with 0.5–2.0% hydrogen peroxide (see Vids. S6 and S7 in the SM [31]). Janus particles may also be synthesized with a thin layer of ferromagnetic material embedded underneath the final catalytic layer [51], such that by encapsulating them in a vesicle, one would ob-

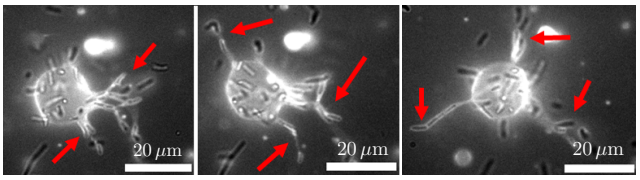

FIG. 4. Experimental images of motile *B. subtilis* contained within a GUV with low bending modulus κ and surface tension λ. When the vesicle is soft, the bacteria generate long membrane tubes upon collision (red arrows). Other than membrane bending stiffness and surface tension, experimental conditions are identical to those of Fig. 1.

tain a fully synthetic, stimuli-responsive lipid membrane vesicle.

In addition to changing the active constituents of a membrane vesicle, one could also investigate vesicles with different membrane properties. In particular, electroformation results in vesicles with a wide range of physical parameters, from which vesicles with specific properties can be selected. Figure 4, for example, shows a vesicle with low bending modulus κ and surface tension λ which contains $\approx$12 motile *B. subtilis* bacteria (see Vid. S8 in the SM [31]). For this set of material parameters, the elastic membrane restoring force cannot balance propulsive bacterial forces, and the bacteria form long, protruding tubes. These membrane tubes, which can be tens of microns in length, persist until the bacteria reorient and swim back towards the vesicle center. Bacteria–membrane systems such as those shown in Fig. 4 may be useful as a synthetic model of an infected mammalian cell: several human pathogens, including *Listeria* and *Shigella*, are known to undergo actin-based motility, deform the cell membrane to form membrane tubes, and tunnel into neighboring host cells [52, 53]. Large membrane shape changes beyond the linear limit have also recently been observed in simulations and experiments [29, 30, 54]; in some cases where $N_{\rm p}\,\tau_{\rm R}/(\tau_{\rm T}+\tau_{\rm R})$ was large, a spherical-to-prolate vesicle shape change was observed. To model such highly nonlinear deformations, the full membrane equations [55] and advanced numerical methods [56] are required.

Acknowledgements.—S.C.T. would like to thank John Brady for valuable support and discussions, Heun-Jin Lee, Rob Phillips, and Mikhail Shapiro for integral support with experiments, and Griffin Chure for generous donation of *B. subtilis* PY79. A.S. would like to thank Kranthi Mandadapu for many stimulating discussions, as well as David Limmer for his feedback on the initial simulations, which were submitted as part of a graduate course at U.C. Berkeley.

S.C.T. acknowledges support from the Miller Institute for Basic Research in Science at U.C. Berkeley. A.S. is supported by the Computational Science Graduate Fellowship from the U.S. Department of Energy, as well as U.C. Berkeley.

* stakatori@ucsb.edu
‡ amaresh.sahu@berkeley.edu

[1] A. Lewis, I. Rousso, E. Khachatryan, I. Brodsky, K. Lieberman, and M. Sheves, Biophys. J. **70**, 2380 (1996).
[2] Z. Bálint, G. A. Végh, A. Popescu, M. Dima, C. Ganea, and G. Váró, Langmuir **23** (2007).
[3] W. Häckl, M. Bärmann, and E. Sackmann, Phys. Rev. Lett. **80**, 1786 (1998).
[4] P. Bieling, T.-D. Li, J. Weichsel, R. McGorty, P. Jreij, B. Huang, D. A. Fletcher, and R. D. Mullins, Cell **164**, 115 (2016).
[5] J.-B. Manneville, P. Bassereau, D. Levy, and J. Prost, Phys. Rev. Lett. **82**, 4356 (1999).
[6] J.-B. Manneville, P. Bassereau, S. Ramaswamy, and J. Prost, Phys. Rev. E **64**, 021908 (2001).
[7] H.-Y. Chen, Phys. Rev. Lett. **92**, 168101 (2004).
[8] N. Gov, Phys. Rev. Lett. **93**, 268104 (2004).
[9] M. A. Lomholt, Phys. Rev. E **73**, 061914 (2006).
[10] L. C.-L. Lin, N. Gov, and F. L. H. Brown, J. Chem. Phys. **124**, 074903 (2006).
[11] B. Loubet, U. Seifert, and M. A. Lomholt, Phys. Rev. E **85**, 031913 (2012).
[12] H. Turlier and T. Betz, "Fluctuations in active membranes," in *Physics of Biological Membranes*, edited by P. Bassereau and P. Sens (Springer International Publishing, Cham, 2018) pp. 581–619.
[13] J. Prost and R. Bruinsma, Europhys. Lett. **33**, 321 (1996).
[14] S. Ramaswamy, J. Toner, and J. Prost, Phys. Rev. Lett. **84**, 3494 (2000).
[15] D. Lacoste and A. W. C. Lau, Europhys. Lett. **70**, 418 (2005).
[16] E. Ben-Isaac, Y. Park, G. Popescu, F. L. H. Brown, N. S. Gov, and Y. Shokef, Phys. Rev. Lett. **106**, 238103 (2011).
[17] L. C.-L. Lin and F. L. H. Brown, Phys. Rev. Lett. **93**, 256001 (2004).
[18] N. S. Gov and A. Gopinathan, Biophys. J. **90**, 454 (2006).
[19] R. Alert, J. Casademunt, J. Brugués, and P. Sens, Biophys. J. **108**, 1878 (2015).
[20] Brochard, F. and Lennon, J.F., J. Phys. France **36**, 1035 (1975).
[21] N. Gov, A. G. Zilman, and S. Safran, Phys. Rev. Lett. **90**, 228101 (2003).
[22] J.-B. Fournier, D. Lacoste, and E. Raphaël, Phys. Rev. Lett. **92**, 018102 (2004).
[23] N. S. Gov and S. A. Safran, Biophys. J. **88**, 1859 (2005).
[24] N. S. Gov, Phys. Rev. E **75**, 011921 (2007).
[25] H. Turlier, D. A. Fedosov, B. Audoly, T. Auth, N. S. Gov, C. Sykes, J.-F. Joanny, G. Gompper, and T. Betz, Nature Physics **12**, 513 (2016).
[26] M. Paoluzzi, R. Di Leonardo, M. C. Marchetti, and L. Angelani, Sci. Rep. **6**, 34146 (2016).
[27] J. Chen, Y. Hua, Y. Jiang, X. Zhou, and L. Zhang, Sci. Rep. **7**, 15006 (2017).
[28] C. Wang, Y.-K. Guo, W.-D. Tian, and K. Chen, J. Chem. Phys. **150**, 044907 (2019).
[29] Y. Li and P. R. ten Wolde, Phys. Rev. Lett. **123**, 148003 (2019).
[30] H. R. Vutukuri, M. Hoore, C. Abaurrea-Velasco, L. van

Buren, A. Dutto, T. Auth, D. A. Fedosov, G. Gompper, and J. Vermant, (2019), arXiv:1911.02381.
[31] See Supplemental Material (SM), which includes experimental videos of passive and active membranes fluctuating, as well as a description of experimental and numerical protocols. The SM additionally cites Refs. [57–60].
[32] M. I. Angelova and D. S. Dimitrov, Faraday Discuss. Chem. Soc. **81**, 303 (1986).
[33] K. Kuribayashi, G. Tresset, P. Coquet, H. Fujita, and S. Takeuchi, Meas. Sci. Tech. **17**, 3121 (2006).
[34] Another possibility is that electroformation temporarily weakens the bacteria, and it takes them time to recover.
[35] Bacterial division occurs on a time scale of ∼30–60 min, and so does not affect our measurements.
[36] J. Pécréaux, H.-G. Döbereiner, J. Prost, J.-F. Joanny, and P. Bassereau, Eur. Phys. J. E **13**, 277 (2004).
[37] R. S. Graci, N. Bezlyepkina, R. L. Knorr, R. Lipowsky, and R. Dimova, Soft Matter **6**, 1472 (2010).
[38] P. Méléard, T. Pott, H. Bouvrais, and J. H. Ipsen, Eur. Phys. J. E **34**, 116 (2011).
[39] We have verified from active particle simulations that small errors in detecting the vesicle center of mass do not significantly affect the results for modes $m \geq 2$.
[40] G. Monge, *Application de l'analyse à la géométrie* (Bernard, 1807).
[41] A. Sahu, A. Glisman, J. Tchoufag, and K. K. Mandadapu, (2019), arXiv:1910.10693.
[42] P. B. Canham, J. Theor. Biol. **26**, 61 (1970).
[43] W. Helfrich, Z. Naturforsch. C **28**, 693 (1973).
[44] E. A. Evans, Biophys. J. **14**, 923 (1974).
[45] K. Sapp and L. Maibaum, Phys. Rev. E **94**, 052414 (2016).
[46] K. Drescher, J. Dunkel, L. H. Cisneros, S. Ganguly, and R. E. Goldstein, Proc. Natl. Acad. Sci. U.S.A. **108**, 10940 (2011).
[47] Our code is publicly available at `https://github.com/mandadapu-group/active-contact`.
[48] W. Yan and J. F. Brady, J. Fluid Mech. **785**, R1 (2015).
[49] N. Nikola, A. P. Solon, Y. Kafri, M. Kardar, J. Tailleur, and R. Voituriez, Phys. Rev. Lett. **117**, 098001 (2016).
[50] S. C. Takatori, R. De Dier, J. Vermant, and J. F. Brady, Nat. Comm. **7**, 10694 (2016).
[51] L. Baraban, D. Makarov, O. G. Schmidt, G. Cuniberti, P. Leiderer, and A. Erbe, Nanoscale **5**, 1332 (2013).
[52] N. Friedrich, M. Hagedorn, D. Soldati-Favre, and T. Soldati, Microbiol. Mol. Biol. R. **76**, 707 (2012).
[53] J. Pizarro-Cerdá, A. Charbit, J. Enninga, F. Lafont, and P. Cossart, Semin. Cell Dev. Biol. **60**, 155 (2016).
[54] M. Fošnarič, S. Penič, A. Iglič, V. Kralj-Iglič, M. Drab, and N. S. Gov, Soft Matter (2019).
[55] A. Sahu, R. A. Sauer, and K. K. Mandadapu, Phys. Rev. E **96**, 042409 (2017).
[56] A. Sahu, Y. A. D. Omar, R. A. Sauer, and K. K. Mandadapu, J. Comp. Phys. **407**, 109253 (2020).
[57] F.-C. Tsai, B. Stuhrmann, and G. H. Koenderink, Langmuir **27**, 10061 (2011).
[58] D. Baird, *Experimentation: An Introduction to Measurement Theory and Experiment Design* (Benjamin Cummings, 3rd Ed., 1994).
[59] P. Méléard, J. Faucon, M. Mitov, and P. Bothorel, Europhys. Lett. **19**, 267 (1992).
[60] L. G. Leal, *Advanced Transport Phenomena: Fluid Mechanics and Convective Transport Processes*, Cambridge Series in Chemical Engineering (Cambridge University Press, 2007).